Prediction of equilibrium water uptake and ions diffusivities in ion-exchange membranes combining Molecular Dynamics and analytical models

Enrico Sireci[a], Giorgio De Luca[b,*], Javier Luque Di Salvo[c], Andrea Cipollina[a,*], Giorgio Micale[a]

[a]*Dipartimento di Ingegneria (DI), Università degli Studi di Palermo – viale delle Scienze Ed.6, Palermo (PA), Italy*

[b]*Institute on Membrane Technology, ITM-CNR, Via P. Bucci 17/C, Rende (CS), Italy*

[c] *INFIQC, Universidad Nacional de Córdoba, Facultad de Ciencias Químicas, Departamento de Química Teórica y Computacional, CONICET, Ciudad Universitaria, X5000HUA Córdoba, Argentina*

Abstract

In recent years, the field of process engineering has witnessed an exponential increase in the usage of ion-exchange membranes (IEM) in light of their pivotal function in green technologies such as electrodialysis (ED), reverse electrodialysis (RED) and fuel cells. One of the key parameters in IEMs performance is the equilibrium water uptake (w_u) as this has been shown to have a prominent effect on some of their fundamental properties such as ionic diffusivities. In this work, we have elaborated a molecular dynamics (MD) protocol to reliably predict the water uptake of IEMs by considering a polysulfone (PSU) functionalized with tetramethylammonium (TMA) anion-exchange membrane (AEM) compensated with chloride anions as case study. The procedure led to good agreement with reported experimental data in a wide range of ion-exchange capacities (IEC) and improved the results with respect to the DFT-based approach developed in our previous work. The issue of considering too thin membrane models compared to the actual IEM was found to be relevant and was addressed by proposing an *ad-hoc* simulation setup; this allowed to reconcile results accuracy with reasonable computational costs. Finally, the computed w_u were used to evaluate chloride counter-ion diffusivities within three different theoretical frameworks (the Mackie-Meares, Yasuda-Lamaze-Ikenberry and Manning-Meares models) and it was found that a satisfactory agreement with experiments can be achieved. This confirmed the potential of the current strategy to predict the w_u and ion diffusivities in IEM without resorting to experimental data, thus paving the way towards a computationally driven design of new membranes.

Corresponding authors (*): G. De Luca, g.deluca@itm.cnr.it; A. Cipollina, andrea.cipollina@unipa.it

Keywords: ion exchange membranes, water uptake, ionic diffusivitiy, Molecular Dynamics, analytical models

1. Introduction

Homogeneous monopolar ion exchange membranes (IEM) are dense polymeric materials that have fixed charged groups covalently attached to their backbone. Ion transport in IEMs is highly selective due to the presence of fixed charges that tend to repel ions with the same charge sign as theirs. This behavior makes these materials appealing for numerous green economy applications such as electrodialysis (ED) for water desalination and wastewater treatment [1–3], reverse electrodialysis (RED) for harvesting energy from salinity gradients [4–6], and fuel cells [7–9].

When the membrane is soaked in an aqueous solution, it absorbs the solvent in a quantity proportional to the concentration of fixed charges they contain. This arises from the strong electrostatic interactions between the charged groups and the polar water molecules [10–12]. The water content is a critical property of IEMs as it has major effects on the overall efficiency of the processes in which they are employed [13–15]. In particular, the membrane water uptake (w_u), namely the mass of water absorbed per unit mass of polymer, has been shown to drive an intrinsic permselectivity-conductivity tradeoff in IEM [16,17]. If on the one hand mounting presence of water inside the membrane contributes to weaken the Donnan exclusion, ultimately leading to reduced permselectivity [18,19], on the other it favors ions transport inasmuch they almost exclusively diffuse through the aqueous phase formed upon water sorption rather than through the polymer network; it follows that, with increasing water content, the movement of ions is enhanced, generally leading to higher ions diffusivities (conductivity) in highly swollen membranes [20,21].

Despite its proven relevance, in most computational studies the w_u is considered as an adjustable parameter or experimental data are relied upon to build the models; although this is a rather convenient procedure, it also causes the modelling to partially loose its predictive power. In our previous articles [22,23], we had developed a DFT-based approach aimed at predicting *ab initio* this quantity, namely without resorting to experiments or adjustable parameters. Albeit the approach represented a significant improvement in comparison to the state-of-the-art, it is also intrinsically not capable of capturing some of the physical responses of the polymer membranes. In particular, the DFT approach predicts a constant number of water molecules per fixed charged group, expressed by the membrane hydration number (λ), regardless of the ion exchange capacity (IEC) of the membrane, that is the concentration of fixed charges in the polymer (generally expressed in mmol per g of dry membrane). However, with increasing IEC, the average distance between functional groups in the membrane becomes smaller and thus the clusters of water molecules coordinated by a single charged group tend to merge, eventually forming actual water pockets within the polymer matrix [24]. Therefore, the w_u is not simply the product of the water molecules that an isolated charged group would coordinate times the total number of charged groups, but it also includes a surplus due to the formation of the water pockets, that becomes more relevant with increasing IEC. Experimental observations confirm this mechanism by showcasing larger values of λ with increasing IEC of the polymer membrane [25]. The DFT-based approach, on the other hand, cannot capture this behavior as it considers just one monomer of the polymer and not its surrounding environment. Even more importantly, our DFT

calculations were performed at T = 0 K. In our previous study [23], λ was obtained by determining how many water molecules were strongly coordinated to the fixed charge (i.e., that were found within a cutoff distance from it, calibrated in respect to H-bonds obtained from QM calculations) upon DFT geometrical optimizations and this approach led to an overestimation of w_u in respect to experiments for this type of IEM. This was ascribed to the fact that, while appearing firmly bound to the charged group at 0 K, at room temperature some water molecules might escape from the fixed charge coordination shell and thus would not be considered for the calculation of λ. It is worth noting that the water molecules escaping from the DFT coordination shell at T = 300 K would not contribute to the calculated global w_u.

Additionally, it is common practice in MD studies of IEM to rely on the mean square displacement (MSD) of chemical species to deduce their diffusivities. Nonetheless, the calculation of MSD trajectories from which diffusivities can be extracted is rather computationally expensive, as long simulations (generally in the order of 10^2 ns) are required to reach the Brownian diffusion regime, which is the precondition for which diffusivities can be rigorously computed from the MSD. Secondly, precautions must be taken for a proper application of this approach [26], leading to the risk that the results are influenced by computational artifacts. In light of these considerations, it would be auspicious that an alternative way to give predictive estimations of ionic diffusivities was found.

The purpose of this article is to propose a novel approach, in which an accurate estimate of the membrane water content obtained computationally is coupled with existing analytical models (the Mackie-Meares [27], Yasuda-Lamaze-Ikenberry [28] and Manning-Meares [29] models) to deduce ionic diffusivities in IEMs. The strategy presented in this work aims at addressing the flaws of the DFT approach mentioned above by employing a new molecular dynamics (MD) protocol and to assess to which extent this strategy is effective in simulating the swelling in water of IEMs and predicting ionic diffusion coefficients. To the best of our knowledge, this is the first computational study that employs MD simulations to predict the w_u in IEM with changing IEC by explicitly modelling the water-membrane interface. This approach, in contrast to the DFT-based methodology, on the one part permits to simulate larger systems thus considering not just a single monomer but a vast chemical environment, and, on the other, to take into account the effect of temperature and pressure. The employment of analytical models allows to deduce, from computational studies carried out at the nanometric scale, a macroscopic property such as diffusivity bypassing the classical yet tricky calculation of the MSD. We are aware that analytical models are not devoid of limitations, but their application is intended here to free the calculation of diffusivities from the inaccuracies that arise from the description of a macroscopic system at the nanometric scale, which is intrinsic of the MD simulations. The diffusivities calculations via analytical models avoid the reproducibility tests involving several simulations boxes necessary to test reproducibility, while cutting dramatically the time allocated to non-equilibrium MD calculations of the MSD. This latter aspect is particularly relevant if predictions of ionic diffusivities in several materials have to be performed.

2. Computational methods

2.1 AEM model

The membrane simulated in this study is composed of a polysulfone polymer backbone fuctionalized with tetramethylammonium (PSU-TMA), whose chemical structure is depicted in Figure 1.

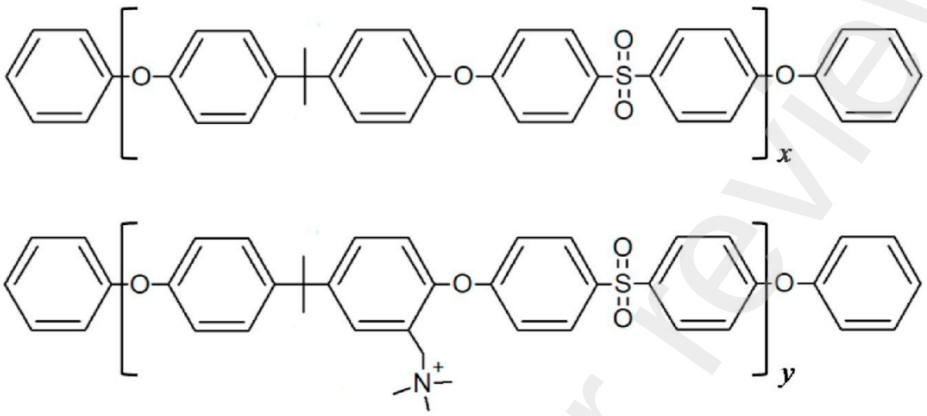

Figure 1. Chemical structure of bare PSU (top) and PSU functionalized with TMA (bottom).

A single polymer chain was made of 157 monomers following the experimental molecular weight of Udel-P1700 polysulfone (69.5 kDa), commonly used in the synthesis of polysulfone-based anion exchange membranes [30–32] . Each membrane model included three identical chains and the IEC was determined by changing the ratio of PSU and TMA-functionalized PSU monomers. The positive charges of the TMA groups were balanced by chloride anions. Uphill of the swelling simulations, the membrane models were equilibrated according to the following procedure based on previous works [33]: (1) an initial steepest descent energy minimization, (2) a 100 ps NVT at 800 K, (3) a 50 ps NVT with temperature decreasing from 800 to 300 K, (4) a 150 ps NVT at 300 K and (5) a 250 ps NPT at 1000 bar and 300 K. Steps (2)-(5) were repeated until a stable response on density was achieved, for which it was generally found that 10-15 of such cycles were necessary. Finally, an 8 ns NPT at 1 bar and 300 K was performed to reach the final structure at ambient conditions. At the start of the equilibration, the box vectors were set in a ratio of 1:1:2 in the *x, y* and *z* directions respectively, so that the final membrane had its *z* dimension 2 times larger than its other dimensions. This was done to enhance the thickness of the membrane which was important to be kept as large as possible. The membrane models with IEC = 0.8, 1.34 and 1.9 mmol/g reached final densities of 1094, 1097 and 1069 kg/m^3, respectively; the models' densities were substantially constant with changing IEC and reasonably close to the experimental value of polysulfone corresponding to 1240 kg/m^3 [34]. The box dimensions were about 5.8X5.8X11.6 nm^3 for all the membranes. Initial configurations of the linear chains were generated with Assemble [35] and MD simulations were performed in GROMACS 2020.4 [36]. Potential forms for the all-atom force field were chosen based on our previous articles [22,23]. Inter- and intra-molecular potential parameters of the polymer were described by the generic Dreiding [37] force field

and the TIP3P model [38] was used to simulate water molecules. The Verlet algorithm with a time step of 1.0 fs, a cutoff for non-bonded interactions of 1.2 nm and a Fourier grid-spacing of 0.1 nm were adopted. The velocity-rescaling Berendsen thermostat with a temperature damping parameter (τ_T) of 0.1 ps, and Berendsen barostat with a pressure damping parameter (τ_P) of 1 ps were used. Periodic boundary conditions were employed in *x, y* and *z*.

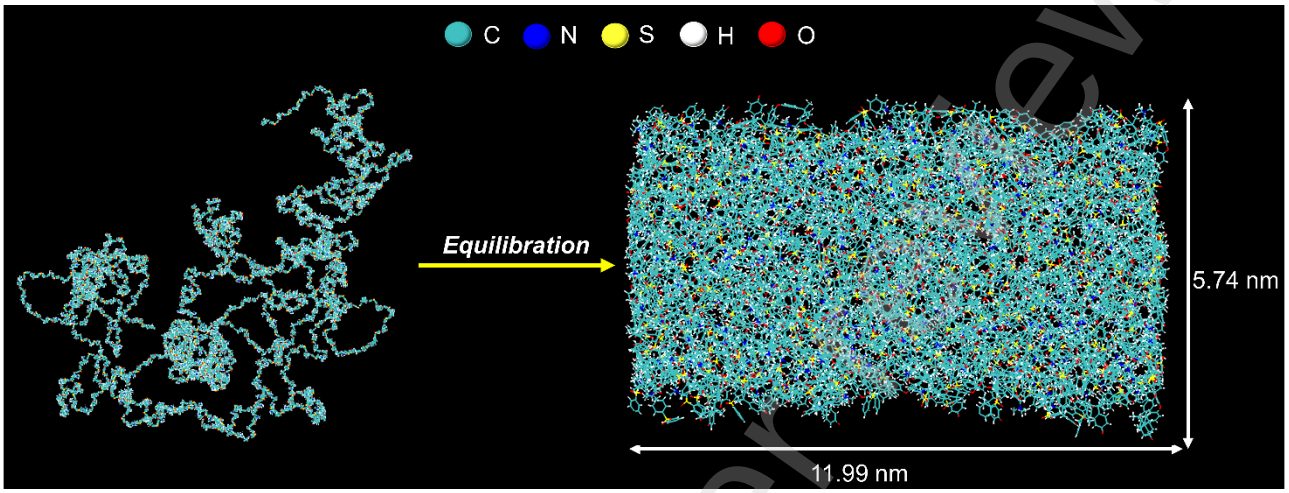

Figure 2. Snapshots of starting polymer configuration generated with Assemble [35] (left) and equilibrated membrane model (right) with IEC = 1.34 mmol/g.

2.2 Swelling procedure

In order to simulate the swelling of the considered systems, two different configurations were adopted. In the first, from now on referred to as "*two-interfaces model*", the equilibrated membrane was interposed in between two water reservoirs. The length of each reservoir was about ¾ of that of the equilibrated membrane. Periodic boundary conditions in all three dimensions were employed for this system. Interposing the membrane in between two reservoirs is the configuration of choice for most previous MD studies of membrane hydration and solvent uptake [33,39–41]. The second model, named "*one-interface model*", showcases the equilibrated membrane in contact with just one water reservoir, whose length was 1.5 times the thickness of the dry membrane. In this setup, periodic boundary conditions were only employed in the x and y directions, while at z = 0 and z = L (where L is the length of the unit cell ~25 nm) two impenetrable 12-6 Lennard-Jones (LJ) walls were placed.

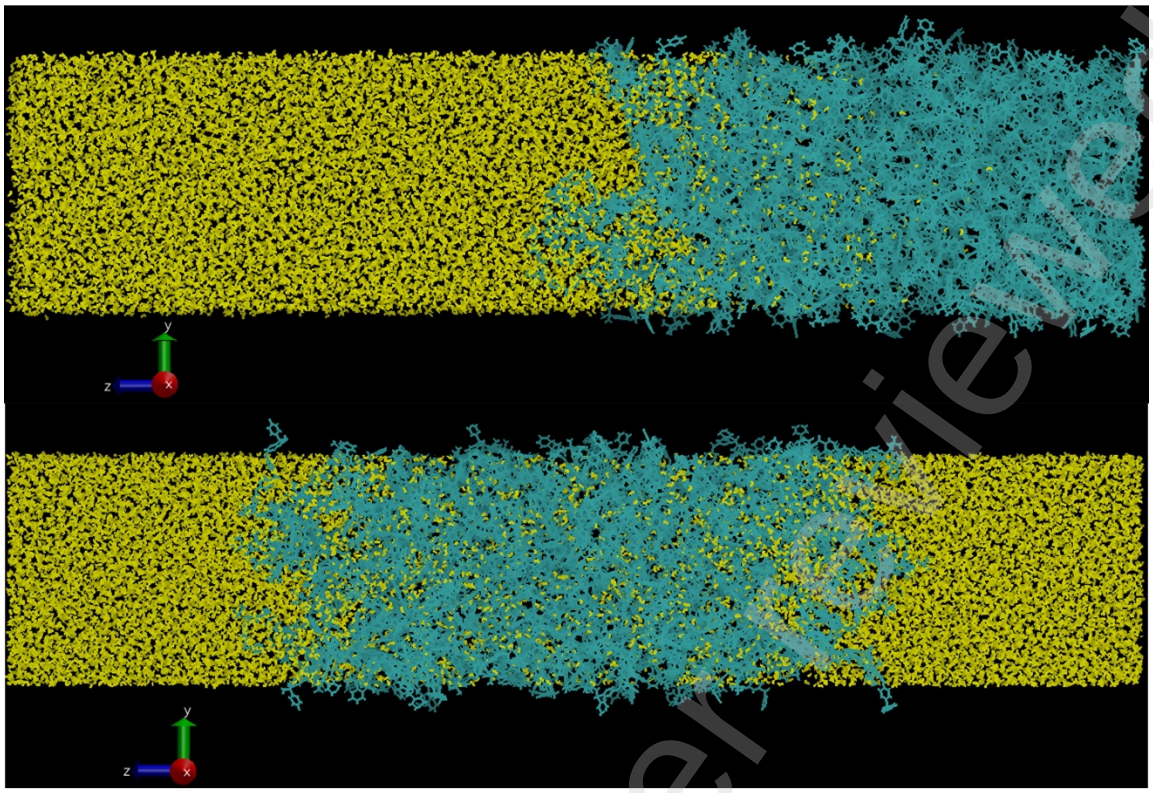

Figure 3. Snapshot of a simulation cell in the *one-interface model* (top) and *two-interfaces model* (bottom).

We employed a swelling protocol based on the one developed by Liu et al. [39] that was successfully applied to mimic the natural swelling of polymer membranes non containing fixed charges. Our protocol consisted in a series of simulated annealing cycles, each involving a 250 ps isothermal and isochoric (NVT, constant number of particles, volume and temperature) MD simulation with a linear temperature ramp from 300 K to 600 K, a 500 ps NVT at 600 K, a 250 ps NVT with a linear temperature ramp from 600 K to 300 K, a 1000 ps NVT at 300 K and a final 500 ps isothermal and isobaric (NPT, constant number of particles, pressure and temperature) simulation at 300 K and 1 bar. During the NPT simulation, semi-isotropic pressure coupling was adopted so that only the z dimension of the simulation box could vary. Since Liu's protocol was formulated for non-charged membranes, precautions had to be taken to successfully apply it to our hydrophilic AEMs' models. In particular, the periodic temperature rise, that served to speed up significantly the process, had to be performed wisely, as we found that, due to the chemical affinity between the two species, the PSU-TMA membranes showed a marked tendency to dissolute in the water reservoirs. For this reason, we limited the temperature rise to T = 600 K instead of T = 800 K as in Liu's original work; additionally, the annealing procedure was halted at the point at which the membrane models reached a hydration equivalent to $\lambda = 8$, and the equilibration cycles only involved a 2000 ps NVT simulation at constant T = 300 K and a subsequent 500 ps NPT simulation at 300 K and 1 bar. As it will be shown later, this prevented the models from overswelling and led to better agreement with experimental data. The choice of the $\lambda = 8$ threshold was motivated by the fact that the experimental reference [25] considered to validate our computational procedure showcased values of λ always larger than 9, and therefore stopping the

annealing cycles from λ = 8 was regarded as a safe choice. At any rate, we believe this does not jeopardize the overall predictive power of the approach as, firstly, most of the commercial IEMs showcase values of λ larger than 8 [42,43], and secondly, it is straightforward to lower the temperature to a constant 300 K earlier or even avoid raising the temperature at all, if needed; nonetheless, this would cause the biphasic models to take much longer to reach equilibrium. This aspect becomes increasingly relevant when larger models, consisting of several polymer chains, are to be equilibrated.

The density profiles of the membrane after each equilibration cycle were extracted from the trajectory of the 500 ps NPT and were fitted using an error function reported in previous works [44] of the form:

$$\rho(z) = \frac{1}{2}\rho_b\left[\mathrm{erf}\left(\frac{z - z_1}{\sqrt{2}\sigma_1}\right) - \mathrm{erf}\left(\frac{z - z_2}{\sqrt{2}\sigma_2}\right)\right] \quad (1)$$

Where ρ_b is the average density of the bulk, z_1 and z_2 are the values of z, that indicate the location of the interfaces, for which the fitting function is equal to $\frac{1}{2}\rho_b$, and σ_1 and σ_2 are the standard deviations that determine how abruptly the function rises to the value of ρ_b. We considered the region of the membrane located between $z = z_1 + 3\sigma_1$ and $z = z_2 - 3\sigma_2$ as the bulk, and the water content was calculated only in this portion. To be noted that in this region the fitting function assumes a value within 99.7% of ρ_b. An illustrative depiction of the fitting explained above is found in Figure 4.

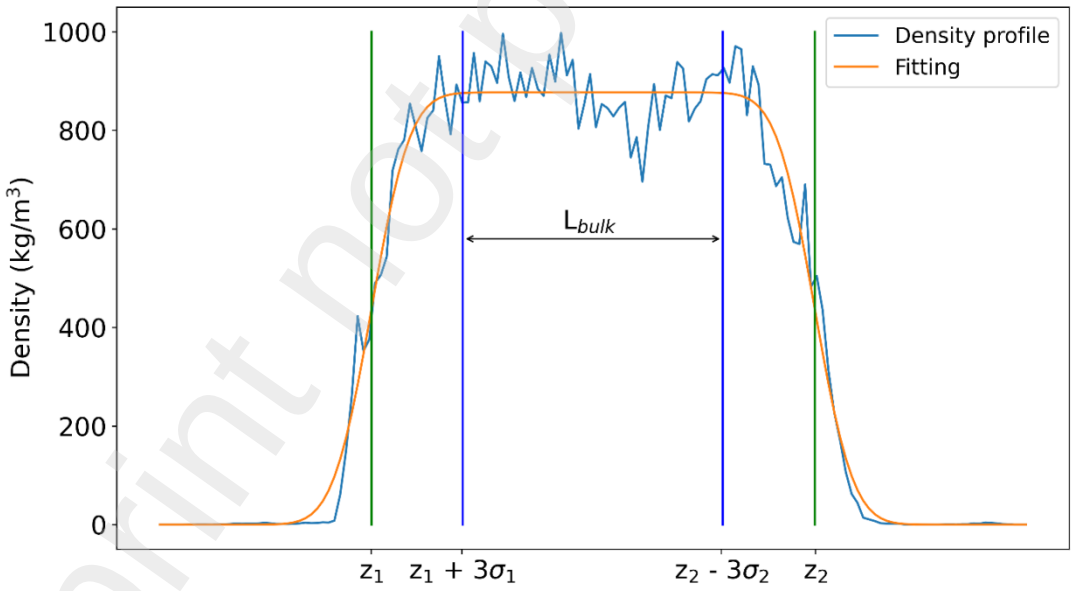

Figure 4. Depiction of a typical density profile and the corresponding fitting function.

The density profiles, such as the one depicted in Figure 4, took into account only the polymer chains and thus the water molecules inside the membrane were considered as voids.

When, in a range of twenty-five equilibration cycles, the variation amplitude of ρ_b was smaller than 1% in respect to the value of ρ_b extracted from the last cycle, the membrane was considered to have reached

equilibrium and the final w_u was extracted from this configuration. For the membrane model with the lowest IEC, due to the reduced slope of the density with increasing number of cycles, this criterium was made more stringent and the difference between the values of ρ_b had to be within a range of 0.75%. The final w_u was calculated by computing the mass of water and that of the polymer in the bulk and by using the following expression:

$$w_u = \frac{m_w}{m_p} \tag{2}$$

Where m_w is the mass of water and m_p is the mass of the polymer. Additionally, λ was calculated using the following formula:

$$\lambda = \frac{w_u}{IEC \cdot M_{H_2O}} \tag{3}$$

Where IEC is the ion exchange capacity expressed in mmol/g and M_{H2O} is the molecular weight of water expressed in g/mmol.

The three different IECs considered in this study were 0.8, 1.34 and 1.9 mmol/g. To assess the influence of the boundary effects on our model, swelling simulations of the membrane with IEC = 1.34 mmol/g were carried out both in the case with one and two interfaces. Since the one-interface model reproduced better the experimental data, only this configuration was considered for the remaining simulations.

During the swelling procedure, the computational details were the same as those presented in Section 2.1 except for the fact that bonds involving hydrogen atoms were constrained and the time step for the Verlet algorithm was 2 fs. The choice of the Berendsen barostat was motivated by the necessity to minimize box length fluctuations that could have had a detrimental effect on the convergence of our model [45].

2.3 Theoretical frameworks for diffusivities calculations

The values of w_u obtained from the MD simulations were further spent to compute chloride counter-ion diffusivities in membrane. To do so, we have employed three different theoretical frameworks widely used for the description of ion diffusion in IEMs, namely the Mackie-Meares [27], the Yasuda-Lamaze-Ikenberry [28] and the Manning-Meares [29] models, whose expressions for calculating the ion diffusivities are shown in equation 4, 5 and 6, respectively.

$$D^{MAC} = D^0\left(\frac{\varphi}{2-\varphi}\right)^2 \tag{4}$$

$$D^{YAS} = D^0 e^{-b_{YLI}\left(\frac{1-\varphi}{\varphi}\right)} \tag{5}$$

$$\frac{D_g^{MAN}}{D_g^0} = f_u(X,\xi)\cdot\left(1-\frac{1}{3}A(X,\xi)\right)\left(\frac{\varphi}{2-\varphi}\right)^2 + f_c(X,\xi)\cdot\frac{\alpha}{3} \tag{6}$$

D^{MAC} and D^{YAS} are the ion diffusivities predicted by the Mackie-Meares and Yasuda models respectively, D^0 is the ion diffusivity in bulk water, φ is the water volume fraction, b_{YLI} is an adjustable parameter, D_g^{MAN} is the counter-ion diffusivity predicted by the Manning-Meares model, and α is a parameter related to the diffusion of condensed counter-ions. Additionally, the expressions for the fraction of uncondensed counter-ions $f_u(X,\xi)$, condensed counter-ions $f_c(X,\xi)$, and the function $A(X,\xi)$ are given below:

$$f_u(X,\xi) = \left(\frac{\frac{X}{\xi}+1}{X+1}\right) \tag{7}$$

$$f_c(X,\xi) = 1 - \left(\frac{\frac{X}{\xi}+1}{X+1}\right) \tag{8}$$

$$A(X,\xi) = \sum_{m_1=-\infty}^{+\infty}\sum_{m_2=-\infty}^{+\infty}\left[\pi\left(m_1^2+m_2^2\right)+1+\frac{2\xi}{X}\right]^{-2} \tag{9}$$

Details on the calculations of the parameter X and the linear charge density ξ are given in the supporting information, whereas m_1 and m_2 are two arbitrary summation indexes. An external NaCl concentration c_{ext} of 0.5 mol/kg was assumed for the calculation of the parameters employed in the Manning-Meares treatment. The double sum in the expression for $A(X,\xi)$ was approximated with a double integral, thus yielding $A(X,\xi) \approx \xi X\left[2+X\left(1+\pi\xi^{-1}\right)\right]^{-1}$. Furthermore, the water volume fraction φ was calculated from the water uptake by using the following formula under the assumption of volume additivity [11,46]:

$$\varphi = \frac{w_u}{w_u + \frac{\rho_w}{\rho_p}} \tag{10}$$

Where ρ_w is the density of water and ρ_p is the density of the dry polymer. The values of ρ_p employed were those obtained upon MD equilibration and before swelling of the membrane. According to Equation S8, ξ is a function of the dielectric constant of the swollen membrane ε, which in turn, according to Equation S9, depends on φ. A brief description of the theoretical frameworks used for diffusivities calculations is given below.

The Mackie-Meares model expresses the ionic diffusivities in polymer membranes as those in the bulk solution corrected by a tortuosity factor; this accounts for the steric hindrance arising from the presence of the polymer chains, that reduce the ionic diffusivities in respect to bulk water. This framework describes the polymer phase as a stationary cubic lattice; additionally, the nature of diffusion in the solution within the polymer phase is not different from that in the bulk solution. It has the advantage of being totally predictive as no adjustable parameters appear in the expression.

The Yasuda model employs a free volume treatment of ions diffusion [47] in polymer membranes. Within this hypothesis, the diffusivity depends exponentially on the free volume (namely, the volume not occupied nor by the polymer neither by water that is included in the bulk volume of the system) which, according to

Yasuda et al., increases linearly with the membrane water content [28,48,49]. Albeit the theoretical backgrounds of the Yasuda and Mackie-Meares models differ from one another, for $\varphi > 0.4$, they have been shown [50,51] to yield an almost identical dependency of ionic diffusivities on the water volume fraction, with the Yasuda model showing better agreement with experiments mostly in light of the parameter b_{YLI} [50]. This quantity, theoretically linked to the size of the diffusing species [28], is generally expressed as an adjustable parameter that is derived by calibrating the model with experimental data. This jeopardizes the predictive nature of the model as it is necessary to resort to experimental data for its application. In this study, the b_{YLI} parameter of the Yasuda model was set equal to 1.8, i.e., the value obtained upon calibration of the analytic model by the MSD-computed diffusivities of our previous work [23].

The Manning-Meares model is the most recent and elaborated among the ones presented here, as it considers both steric and electrostatic effects. The model merges the two effects by considering both a tortuosity factor identical to the one present in the Mackie-Meares description, and an electrostatic one derived by the Manning theory of counter-ion condensation in polyelectrolytes adapted to IEMs. Besides including the assumptions of the Mackie-Meares model, this framework also considers the co- and counter-ions as point charges and the polymer chains as a series of linear point charges. The model is totally predictive for co-ion diffusivities and partially predictive for counter-ion diffusivities. This is due to the current lack of an expression for the parameter α in Equation 6 that, also in this case, must be calibrated experimentally. Herein, this quantity was set to 0; this approximation, used in previous studies [52–54] mentioned by Kitto et al. [51], is quite strong but can still be considered a starting point for a predictive discussion. Nevertheless, current effort in our group is devoted to find a way to give a predictive estimate of this parameter.

The Mackie-Meares framework is valid for homogenous membranes (which is an assumption in the original derivation of the model [27]) and generally leads to poor predictions when low water volume fractions are considered, as in this case the water domains are smaller and the electrostatic ions-membrane interactions are not negligible [49,55,56]. The Yasuda model has been shown to lead to good agreement with experimental data in a wide range of φ ($0.1 < \varphi < 0.8$) [21,57,58] for several commercial IEMs, provided that the membrane structure is homogenous. In fact, structural heterogeneity in the membrane domains, especially relevant when the membranes are mechanically reinforced, has been shown to compromise the validity of the free volume approach of the Yasuda model [14]. As the Manning-Meares model incorporates the Mackie-Meares tortuosity factor, it follows that it is also mostly valid for homogenous membranes. The model is quite recent and, so far, it has been applied to predict ion diffusion in highly swollen IEMs with excellent results [59,60], even though the predictions were less accurate when the co-ion formed complexes with the polymer [60].

3. Results and discussion

3.1 Comparison between the one- and two-interfaces models

The two configurations for the swelling simulations presented in Figure 2 were tested to assess the influence of boundary effects. This was considered worth investigating as we expect the water content in polymer membranes not to be uniformly distributed, but higher in the regions closer to the water-polymer interface and gradually decreasing as we approach the inner portions of the membrane, until it reaches a plateau that corresponds to the w_u observed macroscopically. Since MD simulations typically cover length scales of 10^0-10^1 nm whereas IEMs are generally 100 μm thick, a MD study aimed at predicting water absorption in polymer membranes intrinsically involves the risk of capturing the w_u of the intermediate, more hydrated, region of the membrane rather than that of the bulk. To support this idea, previous experimental studies report a marked increase in w_u when the thickness of polyamide nanofilms goes below ~ 8 nm [61]. As our equilibrated membranes, due to computational limitations, were in the order of 10 nm thick, it was necessary to assess whether the reduced thickness of the modelled membrane with respect to the actual IEM caused the simulations to diverge from experimental results. In the case with one interface, the inner regions of the membrane are further away from the water reservoir compared to the *two-interfaces model*. Let us note that this configuration resembles a thicker membrane without adding any computational cost, as the number of atoms and the dimensions of the unit cell are approximately the same in the two cases.

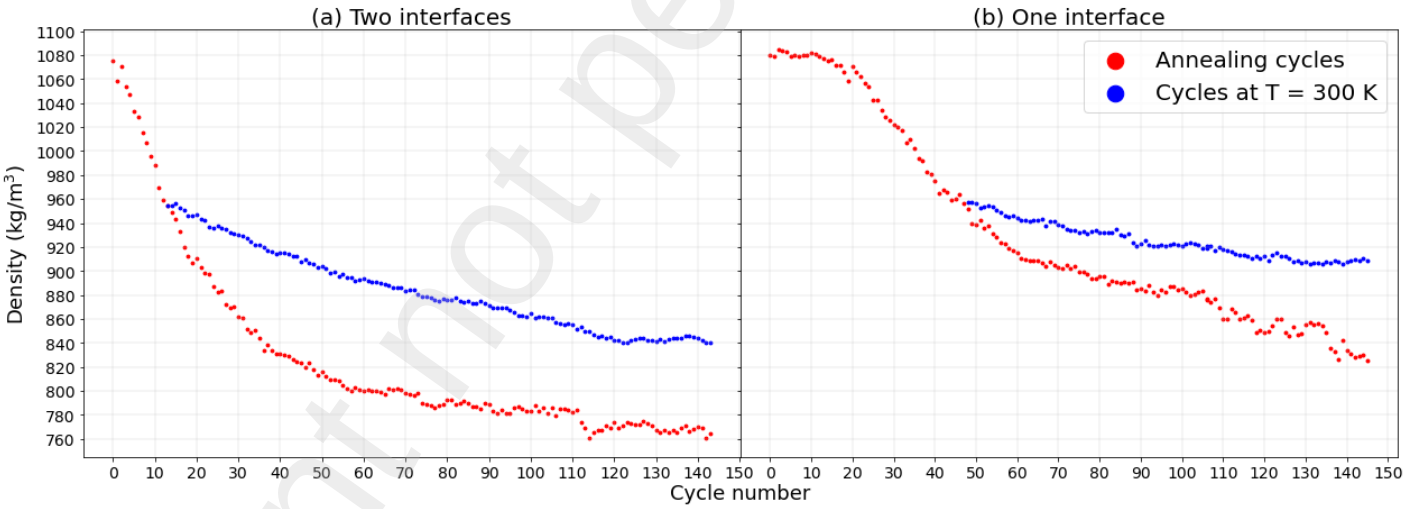

Figure 5. Bulk density evolution with number of equilibration cycles for a model with IEC = 1.34 mmol/g in the two- (a) and one-interface (b) configurations.

In Figure 5, we report the density evolution with the number of cycles of a PSU-TMA membrane with IEC = 1.34 mmol/g in the two configurations, both when the annealing cycles are kept throughout the entire procedure and when they are stopped at λ = 8. Marked discrepancies are recorded for both configurations depending on the extent of the annealing cycles.

Firstly, we detect a significant decrease in the slope of the curves when the annealing cycles are switched off, in agreement with the expectation that the temperature rise during the NVT simulations contributes to speed

up the water absorption. Besides, the two procedures not only affect the swelling kinetics, but also the equilibrium w_u, which increases with decreasing polymer density.

More in detail, in the two-interface model, we observe that the density profile relative to the annealing cycles decays steeply until it reaches a pseudo-plateau around the 100th cycle, followed by a drop and a subsequent final pseudo-plateau (red circles, Figure 5a). In contrast, the density profile (blue circles, Figure 5a*)* obtained through the proposed protocol, which halts the annealing cycles when a water content corresponding to $\lambda = 8$ is achieved, is remarkably different. In fact, it shows a somewhat linear decrease until the 115th cycle, where it stabilizes around a plateau corresponding to a density of 850 kg/m^3, well above the one reached with the annealing cycles only. To be noted that the pseudo-plateaus obtained by only employing the annealing cycles do not satisfy the convergence criterium established in Section 2.2 due to oscillations, whereas the novel protocol leads to a stable plateau that does so between cycles 115th and 145th.

Concerning the one-interface configuration, after an initial steep decay, the density, albeit with a milder slope, keeps decreasing and no plateau is univocally found (red circles Figure 5b). Conversely, the profile obtained with the novel protocol (blue circles Figure 5b*)* portrays a marked decrease in slope upon switching off the annealing cycles followed by a plateau around a density of 910 kg/m^3, above the profile obtained by not stopping the annealing cycles, similarly to the two-interface simulation.

We can conclude that, for hydrophilic IEMs, while raising the temperature during the NVT simulations might accelerate the swelling process, it also induces the membrane models to absorb indefinitely more water. By contrast, when the annealing cycles are interrupted, the membrane stops absorbing water and stable plateaus corresponding to lower w_u can be found in reasonable computational times. Larger water uptakes with increasing temperatures, as recorded in this study when the annealing is adopted, are expected and documented in the literature [62–64].

Furthermore, we report a significant difference between the two configurations in terms of equilibrium degree of hydration obtained using the novel protocol, as in the case with two interfaces the membrane model reaches a w_u of 37.4% ($\lambda = 15.5$) against a value of 27.2% ($\lambda = 11.3$) obtained in the case with only one interface. The larger hydration recorded when the membrane is in contact with two reservoirs supports the idea previously exposed that, at the nanometric scale, the distance between the center of the membrane and the interfaces might not be large enough to capture the bulk properties of the actual IEMs. Since the w_u obtained from the one-interface model is very close to the experimental value of 27% [25], we speculate that, by employing this simulation setup, we were able to mitigate the dimensions-related limitations of our model. However, if this procedure was to be applied to predict the swelling of a membrane not previously characterized experimentally, it would be appropriate to perform an analysis in which the number of polymer chains is gradually increased along with the computational cost. In such case, the increased computational times might be reduced by using coarse-grained models [65] on the one-interface configuration.

We also report two different shapes of the density change rates between the two models. While in the case with one interface the density orbits around the same values during the first 15-20 cycles and starts decreasing afterwards, in the two-interfaces model it almost immediately starts decreasing with a steep slope. This is because, in the latter case, water molecules can enter through both sides, whereas, in the former, it takes longer for water to reach the inner regions of the model.

3.2 Equilibrium water uptake with changing IEC

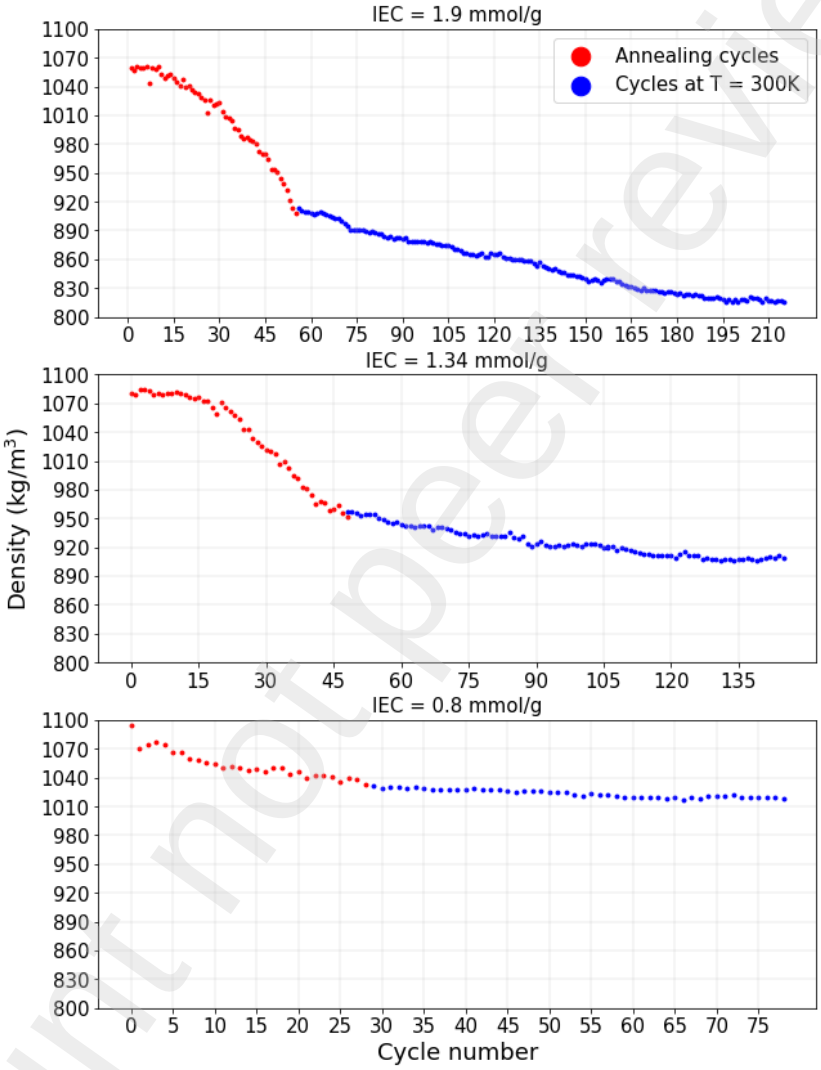

Figure 6. Bulk density evolution with number of equilibration cycles for polymers with IEC (from top to bottom) 1.9, 1.34 and 0.8 mmol/g.

Further swelling simulations of membranes with IEC = 0.8 mmol/g and 1.9 mmol/g were carried out in the one interface model. The choice of this configuration rather than that with two interfaces was motivated by the better agreement with experimental data [25] achieved with this setup when the swelling of the membrane with IEC = 1.34 mmol/g was performed. The density evolutions for all the three IECs investigated are reported in Figure 6. The swelling of the membrane with IEC = 1.9 mmol/g and with IEC = 1.34 mmol/g follow very similar trends: an initial flat region followed by a steep decrease in density that is

drastically reduced upon switching off the heating cycles. During the cycles at 300 K, for both membrane models, the density decrease follows a fairly linear fashion with the difference that in the case of IEC = 1.9 mmol/g, as expected, the plateau is found at lower values of densities corresponding to a larger w_u. In the case of the lowest IEC = 0.8 mmol/g, the density tends to decrease from the first cycles with a mild slope, which becomes almost flat as soon as the equilibration cycles at T = 300 K are introduced, in accordance with the fact that the system was already close to equilibrium at λ = 8. As a general consideration, we observe that the number of cycles required for the models to reach equilibrium increases, along with the computational cost, proportionally with the IEC and the w_u.

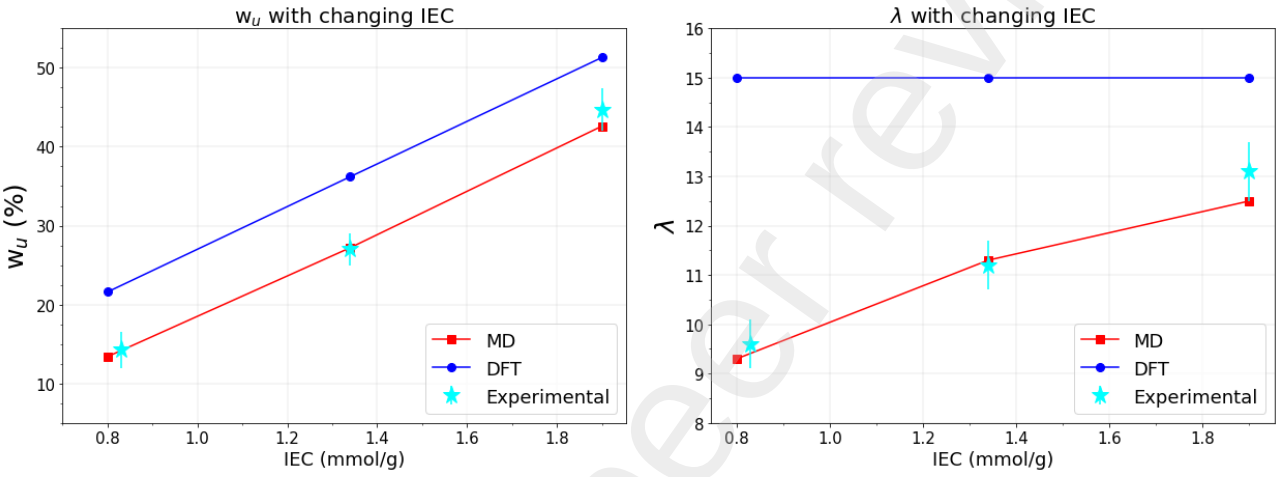

Figure 7. Values of water uptake (w_u) (left) and hydration number (λ) (right) calculated through MD (this article), DFT [23] and reported from experimental works [25].

Overall, the results of the simulations were highly satisfactory as, in all the cases investigated, we produced values of w_u and λ remarkably close to those reported experimentally [25], as it can be observed in Figure 7. Considering the broad range of IEC in which we have carried out our simulations, this can be regarded as strong evidence that the approach presented in this paper is valid for predicting the w_u of IEM. The MD methodology was successful in addressing the flaws of the DFT-based hydration, as, by introducing the effect of temperature, the previously reported overestimation in terms of w_u was overcome as well as the incapability to reproduce increasing values of λ with increasing IEC of the membrane model [23].

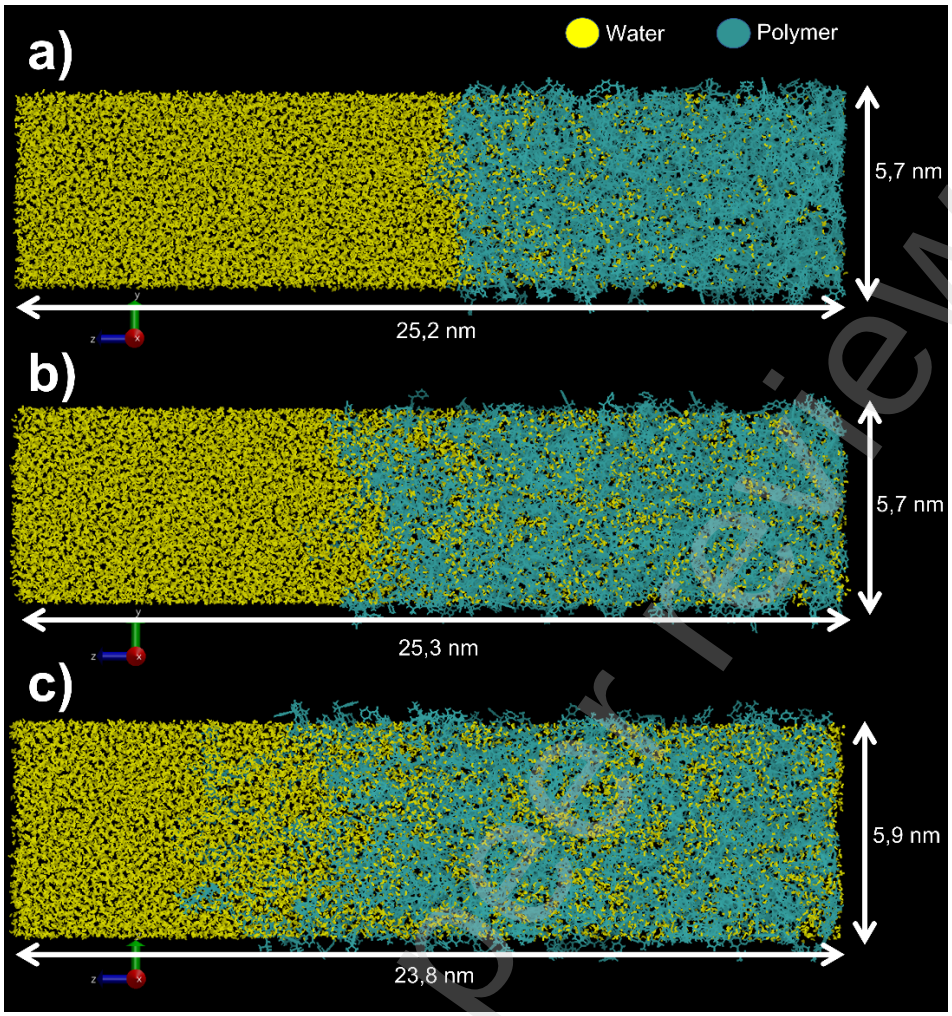

Figure 8. Snapshots of the swollen membranes with IEC = 0.8 (a), 1.34 (b) and 1.9 (c) mmol/g.

Snapshots of the swollen membranes with IEC 0.8, 1.34 and 1.9 mmol/g are presented in Figure 8a-c, respectively. From this figure, it can be clearly observed how the water content increases along with the IEC of the membrane and how the water-polymer interfaces translate gradually in the direction of the water reservoirs. Both aspects are easily rationalized by considering that a larger IEC corresponds to a larger hydrophilicity, this affecting in turn both the w_u of the membrane, its swelling in volume and the consequent tendency of the polymer chains to unravel in the water reservoirs.

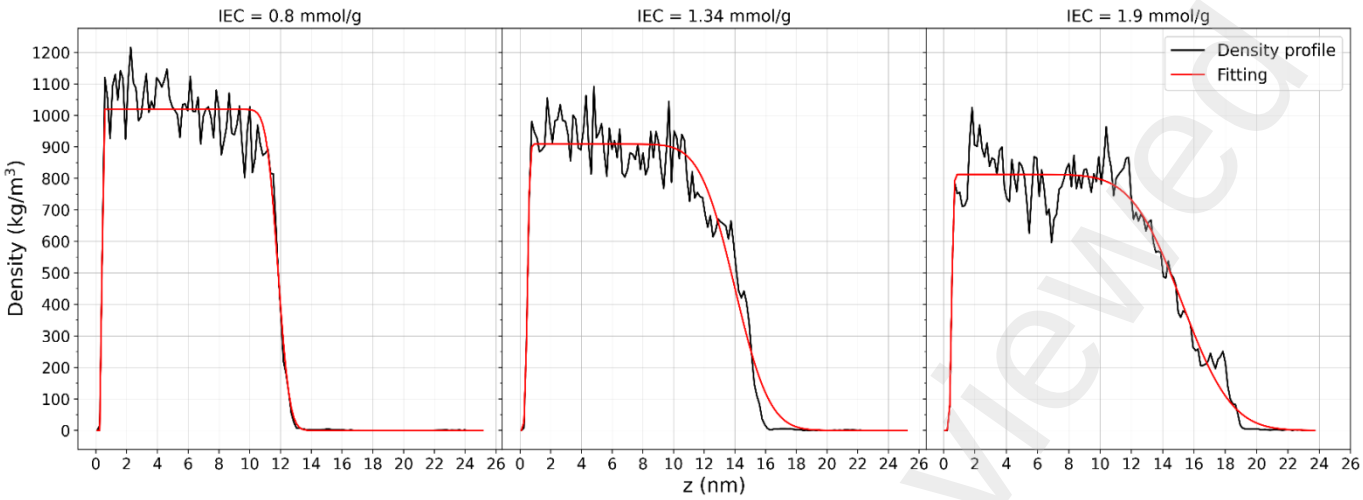

Figure 9. Density profiles and corresponding fitting functions of the swollen membrane models.

Additional quantitative information can be extracted by comparing the density profiles of the different models portrayed in Figure 9. With increasing IEC, the profiles appear more distended, with the bulk density decreasing because of the largerw_u, and the membranes' edge moving forward in the z direction. Furthermore, with increasing IEC, we observe larger transition regions between the membrane and the liquid: while with IEC = 0.8 mmol/g the phase change is rather abrupt and well delimited, with IEC = 1.34 mmol/g and especially IEC = 1.9 mmol/g, we observe density profiles that drop smoothly from the bulk value to 0. This is quantified by the increasing values of the parameter of the fitting functions σ_2, reported, with the others, in Table 3. Recall from Equation 1 that σ_2 is the right standard deviation of the function $\rho(z)$, indicating how abrupt is the transition between the swollen polymer and water phases.

Table 3: Parameters z_1 and z_2 (locations of the interfaces), σ_1 and σ_2 (standard deviations) and ρ_b (average bulk density) of the fitting functions (Equation 1) relative to the equilibrated membrane models with changing IEC.

IEC (mmol/g)	z_1 (nm)	z_2 (nm)	σ_1 (nm)	σ_2 (nm)	ρ_b (kg/m^3)
0.8	0.42	11.8	0.02	0.59	1019
1.34	0.48	14.0	0.12	1.79	909
1.9	0.52	15.2	0.10	2.52	813

The larger extent of the transition region for IEC = 1.9 mmol/g leads us to formulate a computational consideration, namely that, if present, the boundary effects described in Section 3.1 should be more prominent for the largest IEC, i.e., for the most hydrophilic model; for this IEC the risk to not to capture the bulk behavior of the membrane is highest and larger membrane models could be probably used to increase the accuracy of the results.

All in all, the present work suggests that the MD simulations correctly reproduce the effect of the presence of the fixed charges on the membrane properties in relation to the interactions with the solvent, as a neat increasing hydrophilicity, both in terms of morphology and equilibrium w_u, is recorded with increasing IEC.

3.3 Prediction of chloride diffusivity

As anticipated in Section 1, the w_u predicted via the MD simulations was used in a straightforward manner to predict ionic diffusivities. In this section, we computed chloride diffusivities for the membranes with IEC = 0.8, 1.34 and 1.9 mmol/g, whose MD predicted w_u correspond to water volume fractions of 0.125, 0.224 and 0.31, respectively.

The experimental values considered reported by Marino et al. [66] were used for comparison. The Cl^- diffusivities reported by Marino et al. were for a quaternary ammonium functionalized membrane, similar to the one modelled in this paper, with IEC = 2.1 mmol/g and water contents varying between $\varphi \sim 0.05$ and $\varphi \sim 1$. From the w_u obtained upon swelling simulations, we calculated through Equation 10 the above values of φ for which we have predicted chloride diffusivities. Even though the values of φ obtained from the predicted w_u are not equal to those reported by Marino et al., these experimental data should serve as an indication of the trend and orders of magnitude of chloride diffusivities with changing membrane water content.

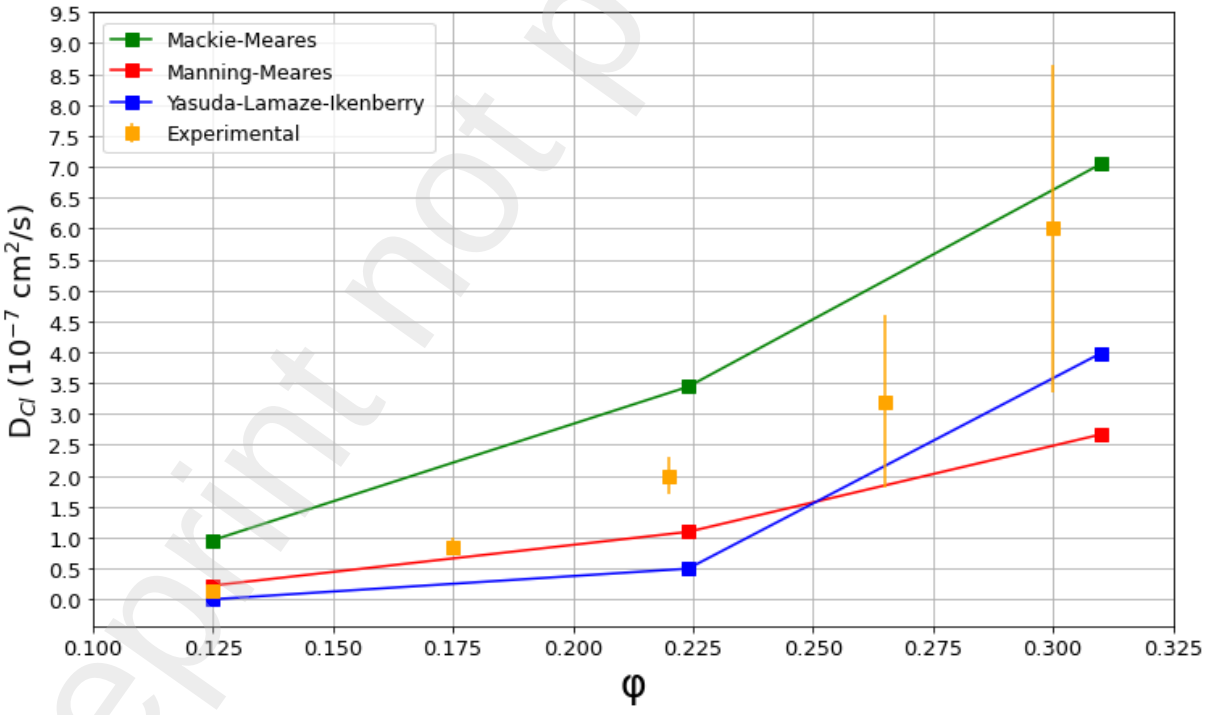

Figure 10. Plot of chloride diffusivities obtained from experiments [66] and three different theoretical frameworks with changing water volume fraction (φ) in the membrane.

As displayed in Figure 10, the Yasuda and the Mackie-Meares models underestimate and overestimate, respectively, the experimental data. Due to the exponential dependency on water volume fraction in the

Yasuda model, the ionic diffusivities tend to zero quite fast in the low water volume fraction region, whereas they rise abruptly for high water contents. Since the investigated water volume fraction range is relatively low, it is expected that the Yasuda model predicts rather low chloride diffusivities; nevertheless, albeit being further from the experimental values in respect to the Mackie-Meares prediction, the treatment within the Yasuda model seems to better reproduce the experimental trend characterized by a steeper slope than the Mackie-Meares one. For this reason, we can expect the Yasuda model to yield better agreement with experiments when the investigated IEM are characterized by larger degrees of hydration. Also, the overestimation delivered by the Mackie-Meares treatment is expected: as explained in Section 2.3, in low water content ranges such as the one investigated, the electrostatic interactions between the membrane and the ions, not considered by the model, are not negligible and cause the predicted diffusivities to be higher than the experimental ones.

The Manning-Meares model yields a good agreement with experiments in the lowest φ region considered in Figure 10, but markedly underestimates chloride diffusivities with increasing water content. Two factors are mainly responsible for this: the first is the electrostatic term (lesser than 1) multiplying the tortuosity term, while the second is the hypothesis that condensed counter-ions were immobile. The latter leads to a significant underestimation of diffusivities: as the predicted percentages of uncondensed counter-ions were 25%, 34% and 41% for IEC = 0.8, 1.34 and 1.9 mmol/g respectively, only a minor part of the ions was considered to contribute to the diffusive mechanism. This underestimation especially causes the diffusivity trend predicted from the model to diverge from the experimental one, as the former is characterized by a rather mild slope in contrast to the more than linear one reported by the latter. Overall, the Manning-Meares treatment involves marked discrepancies with the experimental data, thus confirming the idea reported elsewhere [50,67] that, in fact, condensed counter-ion diffusion should not be neglected as it can play a major role when performing such calculations. Nevertheless, this also means that, among the approaches presented here, the Manning-Meares model has the largest room for improvement.

Overall, we report that the MD approach to predict IEMs' water uptake coupled with theoretical models yields reasonable estimations of ionic diffusivities, all in a predictive fashion and completely bypassing experiments. Moreover, these results are even more encouraging if one considers that they comply with the orders of magnitude of the experimental data and, as far as we are aware, it is the first time that an approach combining numerical computational techniques and analytical models is employed to deduce key operational parameters in IEMs. As a last remark, the values of φ used in the analytical models depend, as shown in Equation 10, on the prediction of the density of the dry polymer ρ_p that involves a certain degree of inaccuracy. However, obtaining a better estimation of ρ_p (employing, for instance, a more accurate force field) would only cause a shift in the values of φ at which the diffusivities were calculated and thus it would not alter the trends reported in Figure 10 and the considerations presented in this section would still be meaningful.

4. Conclusions

A novel strategy that couples MD simulations and theoretical models to predict ionic diffusivities was formulated in this work. The employed simulation protocol was shown to speed up the swelling process without compromising the integrity of the atomistic models. Additionally, an *ad-hoc* simulation setup successfully addressed the dimensions-related limitations of the system without adding computational cost. The MD approach returned values of w_u in very good agreement with experiments and correctly reproduced the experimental trends; moreover, it correctly reproduced the expected increase in hydrophilicity with increasing IEC of the membrane under study, both in terms of water uptake and morphology. Overall, the proposed MD approach represents a new effective way for predicting the water content in IEMs, as it improved the description provided by the DFT strategy developed in our previous works, by adapting to these materials a protocol that was previously employed only for non-charged polymer membranes. It was further shown that the information obtained from the MD simulations could be coupled with existing theoretical models to predict chloride counter-ion diffusivities. Between the three theoretical frameworks investigated, the one developed by Mackie and Meares led to the best results on the grounds of its satisfactory agreement with experimental data reached through a totally predictive approach; this proved that the current methodology can be useful to give preliminary estimations of ionic diffusivities. As a last remark, since we presented in this work a first attempt to predict ions diffusivities via analytic models without resorting to fitting parameters but by calculating the water uptake at the nanometric scale, we believe that rather satisfactory results were achieved.

CRediT authorship contribution statement

Enrico Sireci: Conceptualization, Methodology, Validation, Resources, Data curation, Formal analysis, Investigation, Writing – original draft, Writing – review & editing, Visualization. **Javier Luque Di Salvo**: Conceptualization, Methodology, Validation, Resources, Data curation, Formal analysis, Investigation, Writing – original draft, Writing – review & editing, Visualization. **Giorgio De Luca**: Conceptualization, Methodology, Validation, Resources, Data curation, Formal analysis, Investigation, Writing – original draft, Writing – review & editing, Visualization. **Andrea Cipollina**: Conceptualization, Resources, Data curation, Writing – review & editing, Visualization, Supervision, Funding acquisition. **Giorgio Micale**: Resources, Writing – review & editing, Supervision, Project administration, Funding acquisition.

Declaration of competing interest

The authors declare that they have no known competing financial interests or personal relationships that could have appeared to influence the work reported in this paper.

Acknowledgements

The authors are grateful to SEArcularMINE, H2020 for funding of the project "PRJ-0241" and the support of the CINECA supercomputing center in the frame of the ISCRA project class C MDHIEM (HP10CJPNDM).

Nomenclature and acronyms

Acronym	
AEM	Anion Exchange Membrane
DFT	Density Functional Theory
ED	ElectroDialysis
IEM	Ion Exchange Membrane
IEC	Ion Exchange Capacity
QM	Quantum Mechanical
LJ	Lennard-Jones
MD	Molecular Dynamics
MSD	Mean Square Displacement
NPT	number of particles N, Pressure and Temperature constants (isothermal-isobaric ensemble)
NVT	number of particles N, Volume and Temperature constants (isothermal ensemble)
PSU	Polysulfone
PSU-TMA	Polysulfone-Tetramethylammonium
RED	Reverese ElectroDialysis
TMA	Tetramethylammonium
Symbols	
A	Double sum in electrostatic factor of the Manning-Meares model
b_{YLI}	Parameter of the Yasuda-Lamaze-Ikenberry model
c_{ext}	External NaCl concentration (mol/kg water)
D^0	Self-diffusion coefficient in bulk water (cm^2/s)
D_g^0	Counter-ion self-diffusion coefficient in bulk water (cm^2/s)
D^{MAC}	Self-diffusion coefficient calculated from the Mackie-Meares model (cm^2/s)
D^{YAS}	Self-diffusion coefficient calculated from the Yasuda-Lamaze-Ikenberry model (cm^2/s)
D_g^{MAN}	Counter-ion self-diffusion coefficient calculated from the Manning-Meares model (cm^2/s)
f_c	Fraction of condensed counter-ions
f_u	Fraction of uncondensed counter-ions
w_u	Membrane water uptake
X	Ratio between concentration of fixed charges and salt in membrane
z_1	Location of the left water-polymer interface (nm)
z_2	Location of the right water-polymer interface (nm)
Greek symbols	
α	Parameter linked to condensed counter-ion diffusion
ε	Static dielectric constant of the hydrated membrane
λ	Membrane hydration number
ξ	Dimensionless charge density of the Manning counter-ion condensation theory
ρ_0	Average density of the model bulk during swelling simulations (kg/m^3)
ρ_p	Density of the dry membrane model (kg/m^3)
ρ_w	Density of water (kg/m^3)
σ_1	Left-hand standard deviation of the membrane density fitting function (nm)
σ_2	Right-hand standard deviation of the membrane density fitting function (nm)
τ_T	Temperature damping parameter (ps)
τ_P	Pressure damping parameter (ps)
ξ	Dimensionless charge density of the Manning counter-ion condensation theory
φ	Water volume fraction of the membrane

References

[1] H. Strathmann, Electrodialysis and its Application in the Chemical Process Industry, Separation & Purification Reviews. 14 (1985) 41–66. https://doi.org/10.1080/03602548508068411.

[2] E. Paquay, A.-M. Clarinval, A. Delvaux, M. Degrez, H.D. Hurwitz, Applications of electrodialysis for acid pickling wastewater treatment, Chemical Engineering Journal. 79 (2000) 197–201.

[3] L. Gurreri, A. Tamburini, A. Cipollina, G. Micale, Electrodialysis applications in wastewater treatment for environmental protection and resources recovery: A systematic review on progress and perspectives, Membranes (Basel). 10 (2020) 1–93. https://doi.org/10.3390/membranes10070146.

[4] A. Tamburini, M. Tedesco, A. Cipollina, G. Micale, M. Ciofalo, M. Papapetrou, W. van Baak, A. Piacentino, Reverse electrodialysis heat engine for sustainable power production, Applied Energy. 206 (2017) 1334–1353. https://doi.org/10.1016/j.apenergy.2017.10.008.

[5] H. Tian, Y. Wang, Y. Pei, J.C. Crittenden, Unique applications and improvements of reverse electrodialysis: A review and outlook, Applied Energy. 262 (2020). https://doi.org/10.1016/j.apenergy.2019.114482.

[6] M. Tedesco, A. Cipollina, A. Tamburini, G. Micale, Towards 1 kW power production in a reverse electrodialysis pilot plant with saline waters and concentrated brines, Journal of Membrane Science. 522 (2017) 226–236. https://doi.org/10.1016/j.memsci.2016.09.015.

[7] G. He, Z. Li, J. Zhao, S. Wang, H. Wu, M.D. Guiver, Z. Jiang, Nanostructured ion-exchange membranes for fuel cells: Recent advances and perspectives, Advanced Materials. 27 (2015) 5280–5295. https://doi.org/10.1002/adma.201501406.

[8] G.G. Scherer, Polymer Membranes for Fuel Cells, Ber. Bunsenges. Phys. Chem. 94 (1990) 1008–1014.

[9] R. Souzy, B. Ameduri, Functional fluoropolymers for fuel cell membranes, Progress in Polymer Science . 30 (2005) 644–687. https://doi.org/10.1016/j.progpolymsci.2005.03.004.

[10] H. Ju, A.C. Sagle, B.D. Freeman, J.I. Mardel, A.J. Hill, Characterization of sodium chloride and water transport in crosslinked poly(ethylene oxide) hydrogels, Journal of Membrane Science. 358 (2010) 131–141. https://doi.org/10.1016/j.memsci.2010.04.035.

[11] G.M. Geise, D.R. Paul, B.D. Freeman, Fundamental water and salt transport properties of polymeric materials, Progress in Polymer Science. 39 (2014) 1–42. https://doi.org/10.1016/j.progpolymsci.2013.07.001.

[12] J. Kamcev, D.R. Paul, B.D. Freeman, Effect of fixed charge group concentration on equilibrium ion sorption in ion exchange membranes, Journal of Materials Chemistry A. 5 (2017) 4638–4650. https://doi.org/10.1039/c6ta07954g.

[13] E. Stránská, Relationships between transport and physical–mechanical properties of ion exchange membranes, Desalination and Water Treatment. 56 (2015) 3220–3227. https://doi.org/10.1080/19443994.2014.981413.

[14] R.S. Kingsbury, K. Bruning, S. Zhu, S. Flotron, C.T. Miller, O. Coronell, Influence of Water Uptake, Charge, Manning Parameter, and Contact Angle on Water and Salt Transport in Commercial Ion Exchange Membranes, Industrial and Engineering Chemistry Research. 58 (2019) 18663–18674. https://doi.org/10.1021/acs.iecr.9b04113.

[15] N. Yan, R. Sujanani, J. Kamcev, M. Galizia, E.S. Jang, D.R. Paul, B.D. Freeman, Influence of fixed charge concentration and water uptake on ion sorption in AMPS/PEGDA membranes, Journal of Membrane Science. 644 (2022). https://doi.org/10.1016/j.memsci.2021.120171.

[16] H. Fan, N.Y. Yip, Elucidating conductivity-permselectivity tradeoffs in electrodialysis and reverse electrodialysis by structure-property analysis of ion-exchange membranes, Journal of Membrane Science. 573 (2019) 668–681. https://doi.org/10.1016/j.memsci.2018.11.045.

[17] G.M. Geise, M.A. Hickner, B.E. Logan, Ionic resistance and permselectivity tradeoffs in anion exchange membranes, ACS Applied Materials and Interfaces. 5 (2013) 10294–10301. https://doi.org/10.1021/am403207w.

[18] G.M. Geise, H.S. Lee, D.J. Miller, B.D. Freeman, J.E. McGrath, D.R. Paul, Water purification by membranes: The role of polymer science, Journal of Polymer Science, Part B: Polymer Physics. 48 (2010) 1685–1718. https://doi.org/10.1002/polb.22037.

[19] G.M. Geise, L.P. Falcon, B.D. Freeman, D.R. Paul, Sodium chloride sorption in sulfonated polymers for membrane applications, Journal of Membrane Science. 423–424 (2012) 195–208. https://doi.org/10.1016/j.memsci.2012.08.014.

[20] G.M. Geise, C.M. Doherty, A.J. Hill, B.D. Freeman, D.R. Paul, Free volume characterization of sulfonated styrenic pentablock copolymers using positron annihilation lifetime spectroscopy, Journal of Membrane Science. 453 (2014) 425–434. https://doi.org/10.1016/j.memsci.2013.11.004.

[21] H. Yasuda, C.E. Lamaze, A. Peterlin, Diffusive and Hydraulic Permeabilities of Water in Water-Swollen Polymer Membranes, Journal of Polymer Science: Part A-2. 9 (1971) 1117–1131.

[22] J. Luque Di Salvo, G. de Luca, A. Cipollina, G. Micale, Effect of ion exchange capacity and water uptake on hydroxide transport in PSU-TMA membranes: A DFT and molecular dynamics study, Journal of Membrane Science. 599 (2020) 117837. https://doi.org/10.1016/j.memsci.2020.117837.

[23] J. Luque Di Salvo, G. de Luca, A. Cipollina, G. Micale, A full-atom multiscale modelling for sodium chloride diffusion in anion exchange membranes, Journal of Membrane Science. 637 (2021) 119646. https://doi.org/10.1016/j.memsci.2021.119646.

[24] N. Kononenko, V. Nikonenko, D. Grande, C. Larchet, L. Dammak, M. Fomenko, Y. Volfkovich, Porous structure of ion exchange membranes investigated by various techniques, Advances in Colloid and Interface Science. 246 (2017) 196–216. https://doi.org/10.1016/j.cis.2017.05.007.

[25] X. Duan, C. Wang, T. Wang, X. Xie, X. Zhou, Y. Ye, A polysulfone-based anion exchange membrane for phosphoric acid concentration and purification by electro-electrodialysis, Journal of Membrane Science. 552 (2018) 86–94. https://doi.org/10.1016/j.memsci.2018.02.004.

[26] E.J. Maginn, R.A. Messerly, D.J. Carlson, D.R. Roe, J.R. Elliot, Best Practices for Computing Transport Properties 1. Self-Diffusivity and Viscosity from Equilibrium Molecular Dynamics [Article v1.0], Living Journal of Computational Molecular Science. 2 (2020). https://doi.org/10.33011/livecoms.1.1.6324.

[27] J.S. Mackie, P. Meares, The diffusion of electrolytes in a cation-exchange resin membrane I. Theoretical, Proceedings of the Royal Society of London. Series A. Mathematical and Physical Sciences. 232 (1955) 498–509. https://doi.org/10.1098/rspa.1955.0234.

[28] H. Yasuda, C.E. Lamaze, L.D. Ikenberry, Permeability of Solutes through Hydrated Polymer Membranes, Die Makromolekulare Chemie. 118 (1968) 19–35. https://doi.org/10.1002/macp.1968.021180102.

[29] J. Kamcev, D.R. Paul, G.S. Manning, B.D. Freeman, Predicting salt permeability coefficients in highly swollen, highly charged ion exchange membranes, ACS Applied Materials and Interfaces. 9 (2017) 4044–4056. https://doi.org/10.1021/acsami.6b14902.

[30] J.S. Park, S.H. Park, S.D. Yim, Y.G. Yoon, W.Y. Lee, C.S. Kim, Performance of solid alkaline fuel cells employing anion-exchange membranes, Journal of Power Sources. 178 (2008) 620–626. https://doi.org/10.1016/j.jpowsour.2007.08.043.

[31] J. Pan, S. Lu, Y. Li, A. Huang, L. Zhuang, J. Lu, High-Performance alkaline polymer electrolyte for fuel cell applications, Advanced Functional Materials. 20 (2010) 312–319. https://doi.org/10.1002/adfm.200901314.

[32] X. Wang, M. Li, B.T. Golding, M. Sadeghi, Y. Cao, E.H. Yu, K. Scott, A polytetrafluoroethylene-quaternary 1,4-diazabicyclo-[2.2.2]-octane polysulfone composite membrane for alkaline anion exchange membrane fuel cells, International Journal of Hydrogen Energy. 36 (2011) 10022–10026. https://doi.org/10.1016/j.ijhydene.2011.05.054.

[33] Q. Shi, K. Zhang, R. Lu, J. Jiang, Water desalination and biofuel dehydration through a thin membrane of polymer of intrinsic microporosity: Atomistic simulation study, Journal of Membrane Science. 545 (2018) 49–56. https://doi.org/10.1016/j.memsci.2017.09.057.

[34] V.R. Sastri, High-Temperature Engineering Thermoplastics, in: Plastics in Medical Devices, Elsevier, 2010: pp. 175–215. https://doi.org/10.1016/B978-0-8155-2027-6.10008-X.

[35] M.T. Degiacomi, V. Erastova, M.R. Wilson, Easy creation of polymeric systems for molecular dynamics with Assemble!, Computer Physics Communications. 202 (2016) 304–309. https://doi.org/10.1016/J.CPC.2015.12.026.

[36] M.J. Abraham, T. Murtola, R. Schulz, S. Páll, J.C. Smith, B. Hess, E. Lindah, GROMACS: High performance molecular simulations through multi-level parallelism from laptops to supercomputers, SoftwareX. 1–2 (2015) 19–25. https://doi.org/10.1016/J.SOFTX.2015.06.001.

[37] S.L. Mayo, B.D. Olafson, W.A. Goddard, DREIDING: A Generic Force Field for Molecular Simulations, J. Phys. Chem. 94 (1990) 91101. https://pubs.acs.org/sharingguidelines.

[38] P. Mark, L. Nilsson, Structure and Dynamics of the TIP3P, SPC, and SPC/E Water Models at 298 K, The Journal of Physical Chemistry A. 105 (2001) 9954–9960. https://doi.org/10.1021/jp003020w.

[39] J. Liu, Q. Xu, J. Jiang, A molecular simulation protocol for swelling and organic solvent nanofiltration of polymer membranes, Journal of Membrane Science. 573 (2019) 639–646. https://doi.org/10.1016/j.memsci.2018.12.035.

[40] M. Ding, A. Szymczyk, A. Ghoufi, Hydration of a polyamide reverse-osmosis membrane, Journal of Membrane Science. 501 (2016) 248–253. https://doi.org/10.1016/j.memsci.2015.12.036.

[41] Q. Xu, J. Jiang, Computational Characterization of Ultrathin Polymer Membranes in Liquids, Macromolecules. 51 (2018) 7169–7177. https://doi.org/10.1021/acs.macromol.8b01387.

[42] L. v Karpenko-Jereb, N.P. Berezina, Determination of structural, selective, electrokinetic and percolation characteristics of ion-exchange membranes from conductive data, (2008). https://doi.org/10.1016/j.desal.

[43] H. Strathmann, Ion-exchange membrane separation processes, 1st ed., Elsevier, 2004.

[44] W. Wei, J. Liu, J. Jiang, Atomistic simulation study of polyarylate/zeolitic-imidazolate framework mixed-matrix membranes for water desalination, ACS Applied Nano Materials. 3 (2020) 10022–10031. https://doi.org/10.1021/acsanm.0c02004.

[45] X. Deng, Y. Han, L.C. Lin, W.S.W. Ho, Computational Prediction of Water Sorption in Facilitated Transport Membranes, Journal of Physical Chemistry C. 126 (2022) 3661–3670. https://doi.org/10.1021/acs.jpcc.1c09259.

[46] J. Kamcev, D.R. Paul, B.D. Freeman, Ion activity coefficients in ion exchange polymers: Applicability of Manning's counterion condensation theory, Macromolecules. 48 (2015) 8011–8024. https://doi.org/10.1021/acs.macromol.5b01654.

[47] M.H. Cohen, D. Turnbull, Molecular transport in liquids and glasses, The Journal of Chemical Physics. 31 (1959) 1164–1169. https://doi.org/10.1063/1.1730566.

[48] T. Tran, C. Lin, S. Chaurasia, H. Lin, Elucidating the relationship between states of water and ion transport properties in hydrated polymers, Journal of Membrane Science. 574 (2019) 299–308. https://doi.org/10.1016/j.memsci.2018.12.059.

[49] R. Fernández-Prinl, M. Philipp, Tracer Diffusion Coefficients of Counterions in Homo- and Heteroionic Poly(styrenesulfonate) Resins, The Journal of Physical Chemistry . 80 (1976) 2041–2046. https://pubs.acs.org/sharingguidelines.

[50] D. Kitto, J. Kamcev, Manning condensation in ion exchange membranes: A review on ion partitioning and diffusion models, Journal of Polymer Science. (2022). https://doi.org/10.1002/pol.20210810.

[51] M. Galizia, D.R. Paul, B.D. Freeman, Liquid methanol sorption, diffusion and permeation in charged and uncharged polymers, Polymer (Guildf). 102 (2016) 281–291. https://doi.org/10.1016/j.polymer.2016.09.010.

[52] T. Luo, Y. Zhong, D. Xu, X. Wang, M. Wessling, Combining Manning's theory and the ionic conductivity experimental approach to characterize selectivity of cation exchange membranes, Journal of Membrane Science. 629 (2021). https://doi.org/10.1016/j.memsci.2021.119263.

[53] R.S. Kingsbury, O. Coronell, Modeling and validation of concentration dependence of ion exchange membrane permselectivity: Significance of convection and Manning's counter-ion condensation theory, Journal of Membrane Science. 620 (2021). https://doi.org/10.1016/j.memsci.2020.118411.

[54] Z. Zou, L. Wu, T. Luo, Z. Yan, X. Wang, Assessment of anion exchange membrane selectivity with ionic membrane conductivity, revised with Manning's theory or the Kohlrausch's law, Journal of Membrane Science. 635 (2021). https://doi.org/10.1016/j.memsci.2021.119496.

[55] N. Lakshminarayanaiah, Transport Phenomena in Artificial Membranes, CHEMICAL REVIEWS. 65 (1965) 492–565. https://pubs.acs.org/sharingguidelines.

[56] H.W. Osterhoudt, Transport Properties of Hydrophilic Polymer Membranes. The Influence of Volume Fraction Polymer and Tortuosity on Permeability, The Journal of Physical Chemistry. 78 (1973) 408–411. https://pubs.acs.org/sharingguidelines.

[57] W. Xie, J. Cook, H.B. Park, B.D. Freeman, C.H. Lee, J.E. McGrath, Fundamental salt and water transport properties in directly copolymerized disulfonated poly(arylene ether sulfone) random copolymers, Polymer (Guildf). 52 (2011) 2032–2043. https://doi.org/10.1016/j.polymer.2011.02.006.

[58] H. Zhang, G.M. Geise, Modeling the water permeability and water/salt selectivity tradeoff in polymer membranes, Journal of Membrane Science. 520 (2016) 790–800. https://doi.org/10.1016/j.memsci.2016.08.035.

[59] Y. Ji, H. Luo, G.M. Geise, Specific co-ion sorption and diffusion properties influence membrane permselectivity, Journal of Membrane Science. 563 (2018) 492–504. https://doi.org/10.1016/j.memsci.2018.06.010.

[60] Q. Wang, G.Q. Chen, S.E. Kentish, Sorption and diffusion of organic acid ions in anion exchange membranes: Acetate and lactate ions as a case study, Journal of Membrane Science. 614 (2020). https://doi.org/10.1016/j.memsci.2020.118534.

672 [61] Z. Jiang, S. Karan, A.G. Livingston, Water Transport through Ultrathin Polyamide Nanofilms Used
673 for Reverse Osmosis, Advanced Materials. 30 (2018). https://doi.org/10.1002/adma.201705973.

674 [62] Y.S. Li, T.S. Zhao, W.W. Yang, Measurements of water uptake and transport properties in anion-
675 exchange membranes, International Journal of Hydrogen Energy. 35 (2010) 5656–5665.
676 https://doi.org/10.1016/J.IJHYDENE.2010.03.026.

677 [63] C.G. Arges, M.-S. Jung, G. Johnson, J. Parrondo, V. Ramani, Anion Exchange Membranes (AEMs)
678 with Perfluorinated and Polysulfone Backbones with Different Cation Chemistries, ECS
679 Transactions. 41 (2011) 1795–1816. https://doi.org/10.1149/1.3635711.

680 [64] J.T. Hinatsu, M. Mizuhata, H. Takenaka, Water Uptake of Perfluorosulfonic Acid Membranes from
681 Liquid Water and Water Vapor, Journal of The Electrochemical Society. 141 (1994) 1493–1498.
682 https://doi.org/10.1149/1.2054951.

683 [65] M.G. Saunders, G.A. Voth, Coarse-graining methods for computational biology, Annual Review of
684 Biophysics. 42 (2013) 73–93. https://doi.org/10.1146/annurev-biophys-083012-130348.

685 [66] M.G. Marino, J.P. Melchior, A. Wohlfarth, K.D. Kreuer, Hydroxide, halide and water transport in a
686 model anion exchange membrane, Journal of Membrane Science. 464 (2014) 61–71.
687 https://doi.org/10.1016/j.memsci.2014.04.003.

688 [67] J. Kamcev, D.R. Paul, G.S. Manning, B.D. Freeman, Ion Diffusion Coefficients in Ion Exchange
689 Membranes: Significance of Counterion Condensation, Macromolecules. 51 (2018) 5519–5529.
690 https://doi.org/10.1021/acs.macromol.8b00645.

691